



Inducing the formation of a colloidal albumin carrier of curcumin

Konstantina Matskou^{a,b}, Berke Kisaoglan^a, Barbara Mavroidi^c, Maria Pelecanou^c,
Maria Zoumpantioti^a, Ilias Matis^{a,**}, Aristotelis Xenakis^{a,*}

^a Institute of Chemical Biology, National Hellenic Research Foundation, Athens, 11635, Greece

^b Department of Biology, National Kapodistrian University of Athens, Athens, 15701, Greece

^c Institute of Biosciences and Applications, National Center for Scientific Research "Demokritos", Athens, 15341, Greece



ARTICLE INFO

Keywords:

Bovine serum albumin
Homogenization
Non-covalent association
Equimolar protein-binder

ABSTRACT

The administration and delivery of pharmaceuticals faces a variety of well-known obstacles that result in limited biocompatibility and bioavailability. Efforts to improve these properties have often employed serum albumin, primarily due to its inherent biocompatibility and its ability to enhance the circulation times of pharmaceuticals. In this work, we have adapted a nanoparticle-formulation protocol, to produce a protein carrier of curcumin with bovine serum albumin. This was achieved by using a near-equimolar protein:curcumin ratio instead of the abundance of curcumin that would be normally used in a nanoparticle formulation. Photometric and quantitative analysis of this carrier showed an increased curcumin content in the produced aqueous solutions following the homogenization of bovine serum albumin (water) and curcumin (dichloromethane) phases. Albumin fluorescence studies indicated curcumin association near a tryptophan residue, without excluding the possibility of additional sites. Circular dichroism provided strong evidence of this association through the induced circular dichroism effect and showed that the secondary structure of bovine serum albumin was effectively maintained. Overall, this work presented a new means of facilitating the association of increased levels of curcumin with bovine serum albumin, which could potentially be used to generate additional non-covalent albumin carriers for pharmaceutical compounds.

1. Introduction

Enhancing the bioavailability of insoluble drugs in the blood stream remains a major challenge in formulation science and drug delivery. Research on the matter has focused on either increasing the solubility of a compound by chemical modification, or on the design of carriers that indirectly improve the cargo's bioavailability. The latter often involves the formulation of nanoparticles (NP) wherein the compound is encapsulated. Depending on the route of administration, the NP approach might aim to improve drug circulation times or tissue permeability as well, while limiting unwanted effects such as the formation of the protein corona on its surface [1]. Several NP-drug formulations have been approved for clinical application in recent decades, delivering both hydrophobic and hydrophilic drugs; today, a large portfolio of drug-delivery NPs is available [2]. However, clinical translation of a substantial portion of NP-assisted drug delivery systems is often hindered

by toxicity, colloidal instability, the protein corona effect, elimination from circulation, off-target distribution and more [1,3–6]. Efforts to circumvent or reduce the effect of such issues have, on many occasions, employed proteins. For instance, the Transferrin/Transferrin-receptor (Tf/TfR) complex has been used to facilitate NP passage through the blood-brain barrier, in the form of Tf-functionalized NPs [7], Tf-binding NPs [8], TfR-targeting NPs [9]. Likewise, human serum albumin (HSA), or its bovine analogue (BSA), have been used to generate NPs with improved biocompatibility and bioavailability and in certain cases, the ability to accumulate in certain tumors [5,10–16].

More recently, efforts to bypass common complications associated with NP-assisted drug delivery have exploited biocompatible proteins for the formation of drug-protein carriers or complexes. Serum albumin has been extensively utilized to develop such carriers, mainly because of its various binding sites and its ability to increase the binder's circulation time [10,11,17,18]. Its fatty-acid-binding sites have been used to extend

Abbreviations: BSA, Bovine Serum Albumin; CCM, Curcumin; DLS, Dynamic light scattering; CD, Circular Dichroism; n_{BSA} , Mols of BSA; n_{CCM} , Mols of CCM.

* Corresponding author. National Hellenic Research Foundation, Institute of Chemical Biology, 48, Vassileos Constantinou Av., 11635 Athens, Greece.

** Corresponding author.

E-mail addresses: iliasmatis@eie.gr (I. Matis), arixs@eie.gr (A. Xenakis).

<https://doi.org/10.1016/j.jciso.2022.100051>

Received 15 March 2022; Received in revised form 15 April 2022; Accepted 21 April 2022

2666-934X/© 2022 The Authors. Published by Elsevier B.V. This is an open access article under the CC BY license (<http://creativecommons.org/licenses/by/4.0/>).

the circulation times of lipidated incretin peptides [19] and of Detemir, a lipidated insulin analogue that has received approval for commercial use [20]. Furthermore, albumin's free cysteine (Cys34) allows the site-specific covalent bonding of appropriately modified molecules and generation of albumin-drug conjugates [21]. Overall, albumin allows for a variety of methodologies to be used for the *in situ* or *in vitro* association with a target molecule, through conjugation and non-covalent binding, albumin-binding protein domains, nanobodies and more [18]. One of the simpler approaches to generating an albumin carrier entails the protein's inherent affinity for various small hydrophobic molecules with aromatic groups, such as Curcumin (CCM) [18]. Curcumin is a well-characterized binder of albumin that is practically insoluble in water under physiological conditions, and binds BSA via its phenolic rings in the vicinity of the two Trp-containing hydrophobic pockets of BSA [22].

In this work, we have created a BSA carrier of CCM by homogenization of a two-phase system similar to those described in Nanoparticle-Albumin Based (NAB) protocols. NAB protocols involve the homogenization of a two-phase system containing albumin in an aqueous environment and a hydrophobic compound in an immiscible organic solvent. Abraxane is a prominent NAB-paclitaxel formulation, in which HSA interacts with paclitaxel (PTX) and forms intermolecular disulfide bridges due to the shearing forces of homogenization, to create the hydrophilic shell of the NP [15,16,23,24]. Here, as with NAB protocols, we mixed an aqueous phase containing BSA with a dichloromethane phase containing CCM. This two-phase system was then homogenized by sonication, and dichloromethane was evaporated to yield an aqueous product. Critically, our adaptation differed from typical NAB iterations in that a near-equimolar $n_{\text{BSA}}:n_{\text{CCM}}$ ratio was utilized; NAB iterations require an abundance of the hydrophobic compound [23,25]. This differentiation in our approach originated in the observation of samples that were produced with near-equimolar $n_{\text{BSA}}:n_{\text{CCM}}$ ratios, that lacked the turbidity associated with nanoparticle generation [25], rather, presenting a clear aqueous product with a visibly high CCM content. This initial observation prompted our hypothesis that the cause of this high CCM content in an aqueous solution was its association with BSA. As such, this approach would potentially be useful in the non-covalent attachment of increased amounts of CCM to BSA. To limit any conformational and chemical alterations on BSA that could lead to self-association, we chose sonication as a simple and quick homogenization method; BSA has shown resistance to structural alterations, aggregation or disulfide bridge formation when sonicated for short periods of time [26]. We followed-up on our original observation by qualitatively and quantitatively determining the CCM content in the aqueous phase with photometric and HPLC analyses, respectively. BSA-CCM association was investigated by native-polyacrylamide gel electrophoresis (PAGE), tryptophan fluorescence, and by circular dichroism (CD), which was also employed in the detection of alterations in the secondary structure of BSA. Any potential BSA self-assembly resulting from homogenization was examined by native-PAGE and dynamic light scattering. Finally, the effect of different BSA:CCM molar ratios on NP formation versus BSA-CCM association was investigated.

2. Materials and methods

2.1. Chemicals

Fatty-acid-free Bovine Serum Albumin (BSA) Fraction V (>98%) was purchased from PAN Biotech (Aidenbach, Germany). Curcumin (CCM) (>98%) was purchased from Apollo Scientific (Stockport, UK). Dichloromethane (HPLC grade) was obtained from Chem Lab (Zedelgem, Belgium) and Acetonitrile (HPLC grade) was purchased from Thermo-Fisher Scientific (Waltham, USA). Coomassie brilliant blue R250 was obtained from Applichem (Darmstadt, Germany). All aqueous solutions were prepared with ultrapure water (Siemens Ultra-Clear TWF system, Munich, Germany).

2.2. Sample preparation

Lyophilized BSA was dissolved in double-distilled H₂O (ddH₂O), to a concentration of 50 mg/mL. CCM was dissolved in dichloromethane to create stock solutions of 1.1, 2.2 and 4.4 mg/mL. 1 mL of the aqueous BSA solution was mixed with 0.25 mL of a stock CCM solution to achieve $n_{\text{BSA}}:n_{\text{CCM}}$ molar ratios of 1:1, 1:2 and 1:4. In order to maintain the same volume ratio, the sample containing a 1:20 $n_{\text{BSA}}:n_{\text{CCM}}$ ratio was prepared by using a 5 mg/mL BSA solution in ddH₂O and a 550 µg/mL CCM solution in dichloromethane, due to the limit of CCM solubility in dichloromethane. Two-phase systems were vortexed briefly and were either used directly or sonicated for 5- or 10-min time spans, using a BIORUPTOR® Standard sonicator (Diagenode, Denville, NJ, USA). Samples were transferred into a spherical flask and the organic solvent was evaporated in a 30 °C waterbath under vacuum, using a Buchi Rotavapor R110 (Flawil, Switzerland) rotary evaporator. The remaining aqueous solution was collected, and the flask walls were washed with double distilled H₂O, resulting in an aqueous solution of 5 mL. Control samples that did not contain CCM were prepared under the same conditions, with CCM-free dichloromethane vehicle. All samples were centrifuged (16,000 g, 5 min) to remove any insoluble CCM traces prior to evaluation. Experimental determination of BSA concentration after sample preparation was performed with a Pierce™ BCA protein assay kit (Thermo-Fisher Scientific, Waltham, MA, USA).

2.3. Absorbance and fluorescence measurements

Curcumin absorbance was measured at 425 nm for all samples and was used to provide a qualitative estimate of the CCM content in the prepared aqueous solution. Measurements of Trp fluorescence were used to determine the quenching effect of CCM association with BSA. Trp fluorescence was monitored using an excitation wavelength (λ_{ex}) of 290 nm. Fluorescence emission scans were taken for all samples, from 310 to 410 nm. Absorbance and fluorescence measurements were performed with a Safire2 (Tecan, Männedorf, Switzerland) plate reader.

2.4. Curcumin quantification

The CCM content in each sample was determined by HPLC quantification. CCM was recovered by adding dichloromethane in the prepared sample, within a separation funnel. The two phases were mixed until the aqueous phase was colorless. The dichloromethane volume was at least 4-fold greater than the aqueous phase volume, to favor CCM solubilization in the organic solvent and limit its re-association with BSA. Dichloromethane was then evaporated via rotary evaporator (Buchi Rotavapor R110) and CCM was resolubilized with acetonitrile. An acetonitrile/H₂O (60/40) mobile phase was selected, and samples were quantified using an Agilent Eclipse XDB-C18 (4.6 × 150 mm, 5 µm) column in combination with an Agilent 1100 chromatography system (Santa Clara, CA, USA). CCM detection was performed by absorbance measurements at 430 nm.

2.5. Protein electrophoresis

Native polyacrylamide gel electrophoresis (PAGE) was performed on 12% bis-acrylamide gels. A bromophenol-blue-free loading buffer was used, and CCM-containing bands were observed via their characteristic yellow color. The gel was visualized using a UVP ChemiDoc-it² imager (Analytik Jena, Upland, CA, USA) equipped with a grayscale charge-coupled-device (CCD) camera. The gel was subsequently stained with Coomassie brilliant blue R-250 to allow observation of all present protein bands, the potential depletion of BSA as well as determine which protein species corresponded to the yellow-colored bands.

2.6. Dynamic light scattering

A Zetasizer Nano ZS90 (Malvern Panalytical, Malvern, UK) equipped with a He-Ne laser (632.8 nm), using a non-invasive back scatter (NIBS) technology was employed for dynamic light scattering (DLS) studies. Samples were diluted (0.1 mg/mL BSA), and filtered with a 0.45 μm filter, prior to measurement. The filtration step was introduced to remove externally introduced large particles which can hinder the quality of the results.

2.7. Circular dichroism

Following sample preparation, structural studies of BSA solutions (CCM-free, or 1:1, 1:2 and 1:4 $n_{\text{BSA}}:n_{\text{CCM}}$ ratios) were performed with circular dichroism spectropolarimetry (Jasco J-715 spectropolarimeter, Tokyo, Japan) The CD spectra were recorded at 25 °C in the 190–500 nm range, with 0.2 nm step resolution, 50 nm/min speed, 0.5 nm resolution, and 1 mm bandwidth. The protein concentration in the experiments for the far-UV (200–260 nm) and near-UV (260–300 nm) regions was 0.1 mg/mL, and for the recording of induced CD (ICD) in the near-UV region and visible region (380–500 nm), protein concentration was 10 mg/mL. CD spectra are displayed as ellipticity in units of millidegrees (mdeg). Each spectrum is the average of three scans and three independent experiments for each condition. The CD data were analyzed through the OriginPro 9 program and the content of the secondary structure of BSA was calculated through the CDNN software.

3. Results and discussion

A previous study by Gulseren et al. has shown that moderate sonication (i.e. $t < 15$ min at 20 W/cm^2) has a negligible effect on the structure of BSA or its free-sulfhydryl content, and does not lead to oligomerization or aggregation of the protein [26]. Therefore, a water-bath sonicator intended for the treatment of protein and DNA was chosen for sample homogenization, in order to minimize the effect of sonication on BSA.

3.1. CCM absorbance

Absorbance measurements were performed in the aqueous solutions that resulted from homogenization of the aqueous and dichloromethane phases containing BSA and CCM respectively, and the subsequent evaporation of dichloromethane. Any insoluble CCM was removed from the solution by centrifugation. To evaluate the effect of sonication in the resulting CCM content, samples were either non-sonicated or sonicated for 5 or 10 min. Sonication treatments showed a noticeable increase of CCM content in the resulting aqueous solution, compared to samples that were not sonicated, as shown in Fig. 1. Notably, a longer sonication of 10 min did not further increase CCM absorbance, compared to a 5 min sonication step (Fig. 1). Molar ratios ($n_{\text{BSA}}:n_{\text{CCM}}$) also affected CCM absorbance in the produced aqueous solutions. A higher initial concentration of CCM led to increased CCM absorbance in the produced aqueous solution. Remarkably, this concentration dependence was also observed for non-sonicated samples that were otherwise submitted to the same treatment (Fig. 1).

These findings revealed an increase of CCM content in the produced aqueous solution, which stems both from sample sonication and increased initial CCM concentrations. Considering that CCM is practically insoluble in water under room temperature and physiological pH, the main reason for its apparent “solubilization” is most likely an association with BSA, which is facilitated by the sonication process. It was also interesting to observe that the CCM content increased in a CCM-concentration dependent manner in non-sonicated samples, implying a role of the two-phase system in enabling CCM association with BSA.

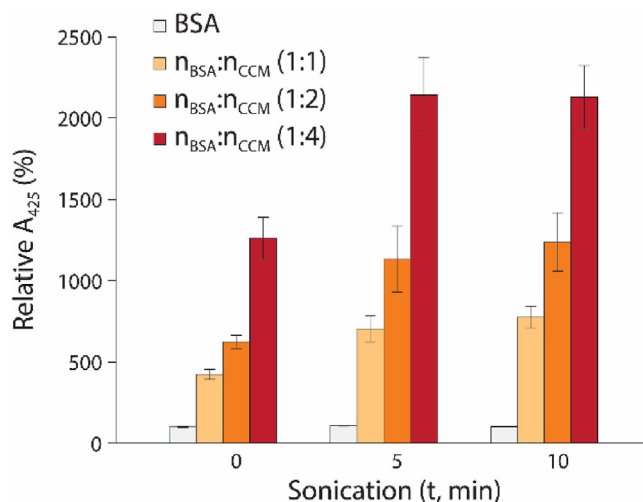


Fig. 1. Curcumin absorbance measurements in the aqueous BSA solution. $n_{\text{BSA}}:n_{\text{CCM}}$ (1:X) indicates molar ratios. Samples labeled as “BSA” did not contain CCM but underwent the same preparation as their CCM-containing equivalents. CCM absorbance was measured at 425 nm to qualitatively determine CCM contents in the aqueous BSA solutions. The absorbance of the non-sonicated BSA ($t = 0$ min) sample was arbitrarily set at 100% to allow normalization of other samples. All absorbance measurements were performed in triplicate ($n = 3$) except for the absorbance measurement of non-sonicated ($t = 0$) BSA ($n = 2$). Error bars represent the standard error of the mean (SEM).

3.2. CCM quantification by HPLC

The increase in CCM content was quantified by analytical HPLC. CCM concentration in the produced aqueous solution (CCM_f) is presented as a percentage of the initial CCM concentration in dichloromethane (CCM_i): $(\text{CCM}_f/\text{CCM}_i) \times 100$ (Fig. 2). Sonicated samples retained more of the initial CCM amount contained originally in the dichloromethane phase, compared to non-sonicated samples, in accordance with CCM absorbance findings. We also observed that sonicated samples with $n_{\text{BSA}}:n_{\text{CCM}}$ ratios of 1:1 and 1:2 could retain most of the initial CCM amount (91% and 80% respectively), while the “1:4” sample retained 47%, not adjusting for sample loss during preparation (80–90% of initial BSA remained in the

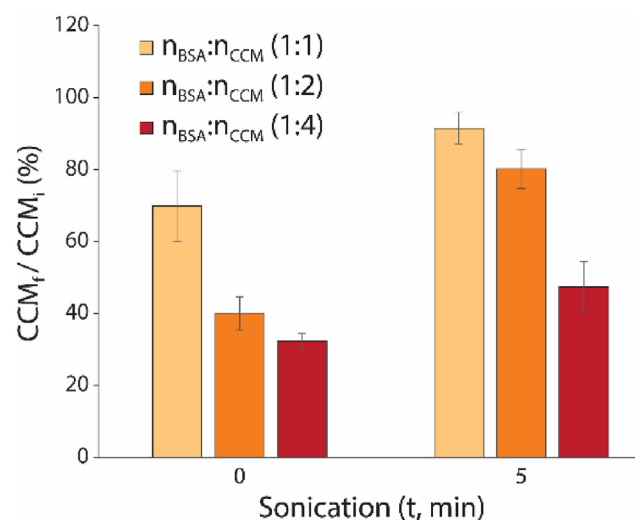


Fig. 2. Curcumin quantification in the aqueous BSA solution by analytical HPLC. $n_{\text{BSA}}:n_{\text{CCM}}$ (1:X) indicates molar ratios. CCM in the aqueous BSA solutions (CCM_f) is presented as a percentage of the corresponding initial CCM concentration (CCM_i). All HPLC quantifications were performed in triplicate ($n = 3$) except for the quantification of sonicated ($t = 5$ min) $n_{\text{BSA}}:n_{\text{CCM}} = 1:4$, ($n = 4$). Error bars represent the standard error of the mean (SEM).

aqueous solution after sample preparation). These results also provide a rough estimate of the number of CCM molecules per BSA in the aqueous solution. Recent studies of BSA have revealed an average of ~ 1 binding sites for CCM [27]. Here, the percentages of retained CCM in sonicated “1:2” and “1:4” samples correspond to CCM:BSA ratios of 1:1.6 and 1:1.9 respectively, in the aqueous preparation. Interestingly, this finding highlights the possibility that more than one molecule of CCM is associated per BSA.

3.3. Investigation of particle size by dynamic light scattering

This study revealed a primary population set with a hydrodynamic diameter (D_h) of ~ 10 nm, present in all samples as well as in CCM-free BSA (Fig. 3). In addition to the centrifugation step described in sample preparation, samples were filtered ($0.45 \mu\text{m}$ filters) as is commonly practiced in DLS protocols to exclude any large particles that were introduced during sample preparation. However, to determine the potential presence of self-assembled BSA species, all samples were also examined without a filtration step (Fig. S1a). Both examinations revealed the presence of populations with $D_h > 100$ nm in intensity spectra, which potentially corresponded to aggregated BSA (Figs. 3 and S1a). Similar populations were present in an unfiltered and unprocessed BSA sample (Fig. S1b) indicating the presence of aggregates formed upon BSA solubilization in water, which is a common finding when using albumin that has not undergone additional purification [28]. An additional population at $D_h \sim 70$ nm, shown more clearly in the examination of unfiltered samples, was present only for sonicated preparations and showed a dependence on the initial CCM concentration (Fig. S1a). This population could potentially indicate the presence of particles that eluded removal by centrifugation, although it is unclear whether these are free-CCM

particles or BSA aggregates. Nevertheless, conversion of intensity-based distributions to number-based distributions, suggests that any species with higher hydrodynamic diameters ($D_h > 70$ nm) formed a small fraction of the total population (Figs. 3 and S1), and that the peaks that appeared at ~ 10 nm constituted the majority of the observable species.

In a study by Falke et al., the hydrodynamic radius (R_h) of BSA has been determined by DLS studies at 3.8 nm in intensity-based distributions ($D_h = 7.6$ nm) [29]. The higher mean hydrodynamic diameters noticed here, at ~ 10 nm, could be attributed to the presence of populations of soluble BSA oligomers, such as dimers and trimers, along with the BSA monomer. This assumption was supported by native-PAGE analysis which clearly revealed the presence of small BSA oligomers in the presence of a dominant BSA monomer (Fig. 4). The presence of such oligomers is thought to be the result of the isolation process of BSA, while the dimers, which comprise the second most abundant population among BSA species (Fig. 4), are considered to be the result of intermolecular disulfide bridges formed by the free sulfhydryl groups of Cys34 [30].

Although the presence of colloidal nanoparticles cannot be dismissed by this evaluation due to the sample centrifugation step after evaporation, none of the near-equimolar $n_{\text{BSA}}:n_{\text{CCM}}$ samples displayed the turbidity commonly observed upon NP formation, especially at such protein concentrations.

3.4. Native-PAGE analysis

Based on a previously published protocol that recommended the use of CCM as a protein stain [31], we hypothesized that it would be possible to visualize CCM-containing species of BSA in native-PAGE, without the need for further staining. CCM-containing bands (Fig. 4, upper gel, shown in grayscale), corresponded primarily to monomeric BSA and to a

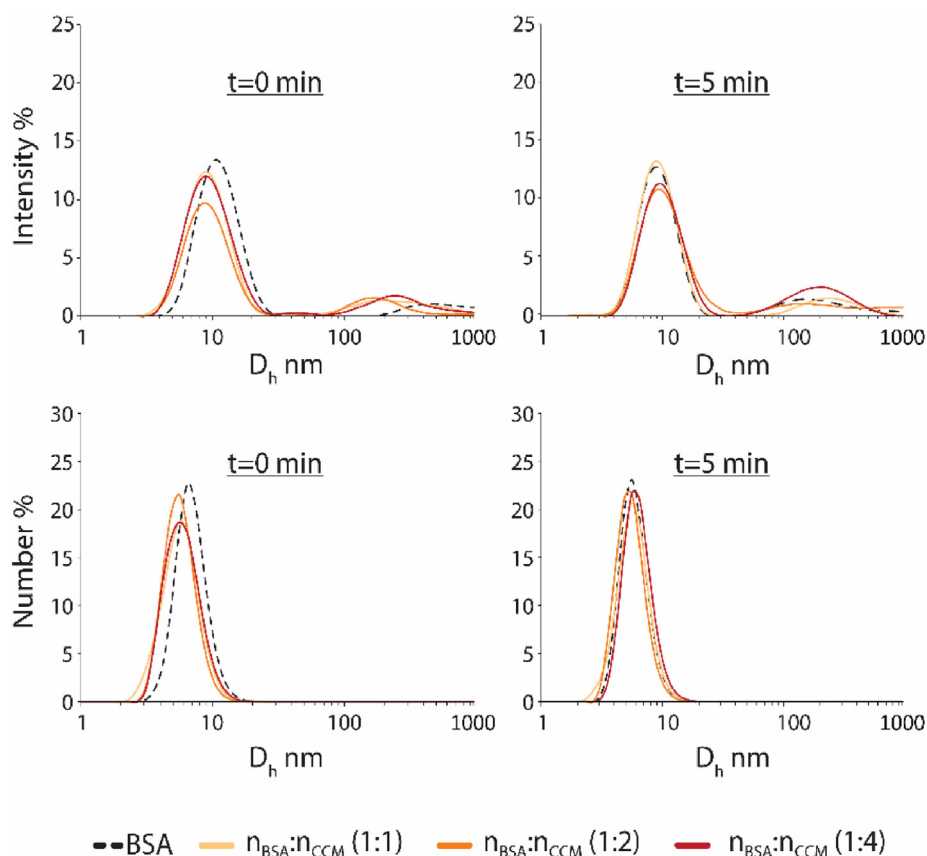


Fig. 3. Particle sizes in the aqueous BSA solutions as determined by dynamic light scattering. $n_{\text{BSA}}:n_{\text{CCM}}$ (1:X) indicates molar ratios. Samples labeled as “BSA” did not contain CCM but underwent the same preparation as their CCM-containing counterparts. Sonication timespans are noted as “t = x min”. Upper spectra correspond to intensity-based distributions and lower spectra correspond to number-based distributions.

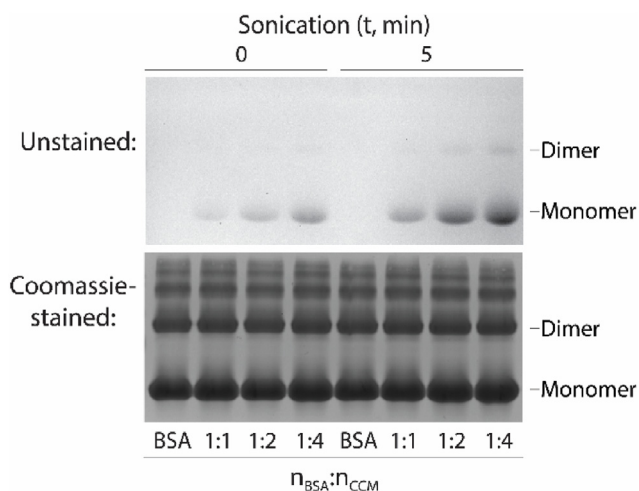


Fig. 4. Native-PAGE analysis of aqueous BSA solutions. $n_{\text{BSA}}:n_{\text{CCM}}$ (1:X) indicates molar ratios. Samples labeled as “BSA” did not contain CCM but underwent the same treatment as their CCM-containing equivalents. Upper image shows the unstained gel. Protein bands were visualized via the yellow color of CCM that was associated with the protein [31] (image was captured with a grayscale imaging system). Lower image: the same gel as in the upper image, following Coomassie-staining.

lesser degree, to BSA dimers, as revealed by the subsequent staining of the gel with Coomassie blue (Fig. 4, lower gel). Sonicated samples showed a visibly increased CCM association for both monomeric and dimeric BSA species. Likewise, band density was dependent on the initial CCM concentration, for both sonicated and non-sonicated samples. Following coomassie-staining, the monomeric and oligomeric BSA bands revealed no changes in protein composition throughout the sample range, indicating no BSA depletion and therefore no further BSA oligomerization and aggregation. The apparent BSA dimer and oligomer species shown in the Coomassie-stained gel were common for all samples (Fig. 4, lower gel). Dimers and other oligomers are likely the result of the isolation process of BSA and have been a common finding in other publications using commercially available BSA [28,30,32,33].

These results imply an association between CCM and BSA, which appears to take place primarily with the monomer. The presence of soluble oligomeric BSA species remains unchanged in the sample set of Fig. 4 while the lack of BSA depletion indicates that no significant aggregation of BSA has taken place post-sample preparation. Equally, BSA-based NPs are not likely a component of the aqueous solution since their generation would have been reflected on the BSA band densities.

3.5. Fluorescence quenching

The effect of CCM association with BSA can be observed by the quenching effect on the protein's intrinsic fluorescence. BSA's main intrinsic fluorophores are found in tryptophan (Trp), tyrosine (Tyr) residues, although its fluorescence is principally attributed to its Trp residues (Trp134 and Trp213) [34,35]. The quenching of Trp fluorescence by a compound that binds to albumin has been employed in the characterization of protein-compound binding [36,37]. In fact, the hydrophobic pockets of BSA containing the tryptophan residues have been proposed to be binding sites for CCM and for two of its derivatives [37]. Tyr fluorophores are also excited at a similar wavelength as Trp fluorophores (280–285 nm), however, excitation of BSA at 280 nm has previously revealed a minimal Tyr contribution when emission was measured at 340 nm [38,39]. Considering all of the above, we expected our observations of sample fluorescence to be associated with Trp and therefore any quenching effects to be the result of CCM association with BSA in the vicinity of a Trp residue.

All samples that contained CCM showed CCM-concentration-dependent quenching of fluorescence (Fig. 5). Following the same pattern observed in previous studies, sonication (Fig. 5, right) further increased the quenching effect. Overall, our results suggest that CCM associates with BSA in the vicinity of a Trp, however, the presence of additional CCM-binding sites cannot be dismissed at this point, requiring further evaluation.

Samples containing CCM also developed a minor blue shift compared to BSA control samples without CCM (Table 1), which indicates that the Trp fluorophore is found in a more hydrophobic environment, consistent with the presence of a CCM molecule [40]. The emission maxima observed for BSA controls without CCM, also coincided with the emission maximum observed for untreated native BSA: $\lambda_{\text{em}} = 354 \text{ nm}$ (Fig. S2).

3.6. Circular dichroism studies

CD spectropolarimetry was employed to study the conformation of BSA in the solutions under study and to acquire evidence for its interaction with CCM. Fig. 6 summarizes the CD spectra of BSA-CCM samples of different molar ratios, with or without sonication. In full accordance with the literature [41], plain BSA exhibits a positive band at 191 nm and two negative bands at 208 nm and 220 nm, characteristic of the dominant α -helical structure of the protein. In addition, quantitative secondary structure analysis of free BSA showed a 61.8% content of α -helix, 21.8% β -sheet and 16.4% random coil in compliance with similar reports [22]. As depicted in Fig. 6a, without sonication, the spectra of BSA remain unchanged in the presence of CCM at the 1:1 and 1:2 $n_{\text{BSA}}:n_{\text{CCM}}$ ratios, while a slight decrease in the negative bands is noted at the 1:4 $n_{\text{BSA}}:n_{\text{CCM}}$ ratio, without any shift in peak position. The decrease in the negative bands is greater when sonication is present, and more intense at increased CCM concentrations (Fig. 6b). In fact, at the 1:4 $n_{\text{BSA}}:n_{\text{CCM}}$ ratio of the sonicated samples, the α -helical structure decreased to 55%, while β -sheet content increased to 28% indicating that CCM binding induces limited uncoiling of α -helices in BSA. Similar changes in helicity of up to 6% have been observed in the literature upon binding of drugs and other compounds to BSA [42,43]. Overall, the CD spectra indicate that in the presence of CCM, α -helix is still dominant, though α -helix to β -sheet transitions are noted with increasing CCM content. The differentiation between non-sonicated and sonicated samples may suggest a more efficient interaction of the BSA with CCM in the sonicated samples.

CD spectra were also obtained in the near-UV and visible range 250–500 nm where CCM absorbs light. As can be seen in Fig. 7, an induced circular dichroism (ICD) signal is present providing strong evidence for the interaction of CCM with BSA [44]. As CCM is a non-chiral molecule with no CD absorption, the generation of ICD attests to the perturbation of CCM symmetry induced by its interaction with the asymmetric BSA environment. CCM bound to BSA, acts as a chiral molecule and generates a bisignate ICD signal, with a negative Cotton band centered at 350 nm, a positive band centered at 425 nm, and a zero-crossover point at 380 nm. A similar ICD spectrum has been reported for HSA in the presence of CCM (1:1 ratio) at pH 7.0 [45] and 7.4 [46]. The intensity of both bands increases with increasing CCM concentration, with no significant change in wavelength position for the negative band or the crossover point, but with a gradual shift for the positive band. At the highest CCM concentration the positive band appears at 458 nm, registering a 33 nm red shift. The increase in intensity of the ICD spectra at the higher curcumin molar ratios reflect the higher fraction of curcumin complexed to BSA.

It is documented in the literature based on fluorescence quenching, CD displacement experiments, and molecular modelling, that the primary binding site of curcumin is the hydrophobic pocket of subdomain IIA of HSA and BSA [47,48]. At the pH = 6.0 of our solutions, the planar π -conjugated phenolic structure of curcumin interacts with BSA through hydrogen bonding and hydrophobic interactions with the aliphatic and aromatic protein side chains [22,45]. Intermolecular exciton coupling between curcumin and the far UV π - π^* transitions of the aromatic side

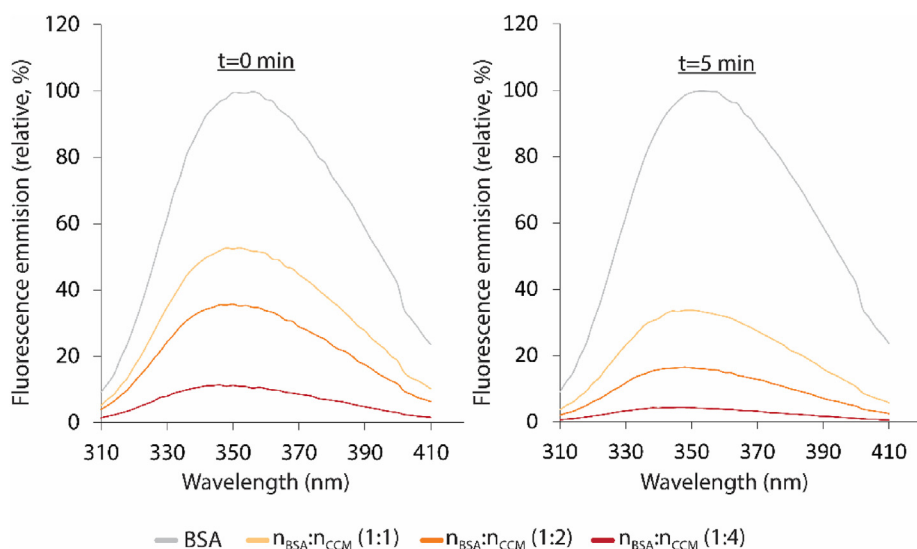


Fig. 5. Tryptophan fluorescence spectra of aqueous BSA solutions following sample preparation. $n_{\text{BSA}}:n_{\text{CCM}}$ (1:X) indicates molar ratios. Samples labeled “BSA” did not contain CCM but were prepared in the same manner as the CCM-containing samples. Fluorescence excitation was fixed at $\lambda_{\text{ex}} = 290$ nm and emission scans were taken between 310 and 410 nm. Samples were normalized using their respective “BSA” control. All fluorescence quenching studies for sonicated samples ($t = 5$ min) were performed in triplicate ($n = 3$), and in duplicate ($n = 2$) for non-sonicated samples ($t = 0$ min).

Table 1

Average BSA emission maxima observed in fluorescence emission scans from 310 to 410 nm ($\lambda_{\text{ex}} = 290$ nm).

		Sonication (t, min)	
		0	5
BSA		356 nm	354 nm
$n_{\text{BSA}}:n_{\text{CCM}}$	(1:1)	352 nm	350 nm
	(1:2)	350 nm	348 nm
	(1:4)	346 nm	348 nm
Native BSA		354 nm	

chains located at the BSA IIA subdomain, may therefore be contributing to the observed ICD signal in our samples [48]. This reasoning is in agreement with the fluorescent quenching experiments (Section 3.5) that support the interaction of CCM with BSA in the vicinity of a Trp. The red shift of the positive band at higher curcumin ratios together with its overall broader shape, may be indicating the presence of a second binding site for CCM that gives positive ICD sign at higher wavelengths and contributes to the generation of a composite positive band. An only-positive ICD signal at approximately 460 nm has been reported for curcumin:BSA interaction at pH 6.4 in the presence of phosphate buffer and for a curcumin:BSA ratio of 0.75 [49]. Furthermore, the presence of a

second binding site for CCM on HSA has been suggested in the literature based on spectroscopic data [45,46].

Overall, the CD studies confirm the stability of BSA secondary structure in the sonicated samples, provide solid evidence for the presence of interaction of BSA with CCM with preservation of the α -helical structure and are in agreement with binding of CCM in subdomain IIA of BSA. Further experimentation is required to delineate the mode of BSA-CCM binding interaction in our samples.

3.7. The role of $n_{\text{BSA}}:n_{\text{CCM}}$ molar ratios

Previous work by Kim et al., has shown that the homogenization of a two-solvent system containing CCM and BSA leads to the formation of NPs with a diameter of ~ 130 nm, when a molar abundance of CCM is used [25]. Here, we investigated the role of near equimolar $n_{\text{BSA}}:n_{\text{CCM}}$ ratios with a modified protocol, showing that CCM associates with BSA and yields a clear aqueous solution rather than a colloidal NP suspension. To verify that the sonication-based homogenization step was capable of yielding NPs when CCM is abundant, we used a $n_{\text{BSA}}:n_{\text{CCM}}$ ratio of 1:20, which promptly resulted in a yellow aqueous suspension (Fig. 8). A lower BSA concentration (5 mg/mL instead of 50 mg/mL used in other ratios) was used in the generation of the “1:20” sample to maintain the water/dichloromethane volume ratio, due to limitations set by CCM

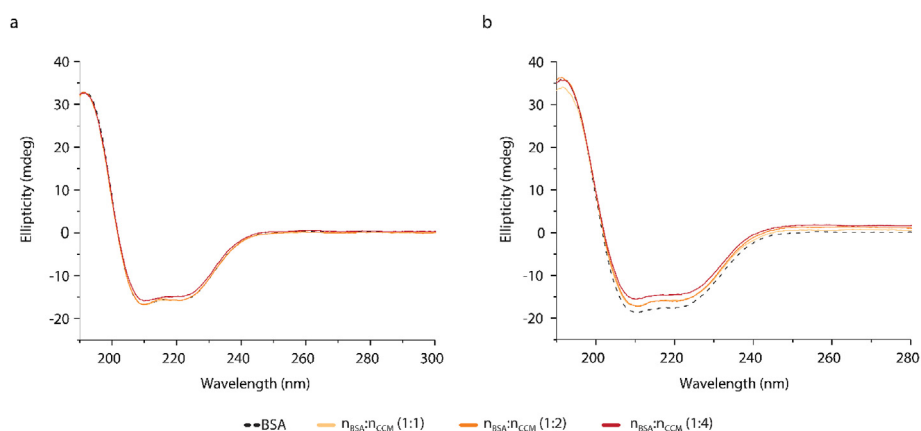


Fig. 6. Secondary structure of BSA upon interaction with CCM following sample preparation. CD spectra of BSA (0.1 mg/mL), pH 6.0, at 25 °C in the absence or presence of CCM at different $n_{\text{BSA}}:n_{\text{CCM}}$ ratios (1:1, 1:2 and 1:4) without (a) or with (b) sonication (5 min). Representative spectra from $n = 3$ independent experiments are presented.

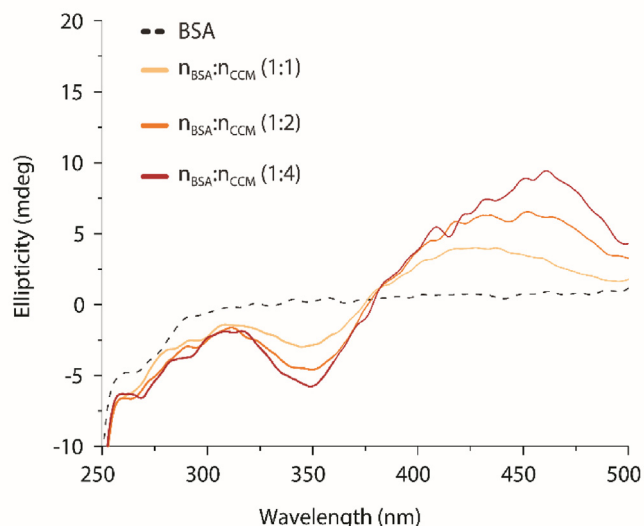


Fig. 7. Induction of circular dichroism signal in CCM upon interaction with BSA after sample preparation. ICD spectra of BSA (10 mg/mL) at 25 °C and pH 6.0 in the absence or presence of CCM at different $n_{\text{BSA}}:n_{\text{CCM}}$ ratios (1:1, 1:2 and 1:4) with 5 min sonication. Representative spectra from $n = 3$ independent experiments are presented.

solubility in dichloromethane. DLS measurements corroborated the existence of NPs in the “1:20” sample by revealing populations of particles with $D_h \sim 350$ nm (Fig. S1c). The larger size of obtained NPs compared to those produced by Kim et al. [25], could be explained by the use of sonication instead of a high-pressure homogenizer [23].

The use of near equimolar ratios yielded clear aqueous solutions as shown in Fig. 8, which also highlights the discussed CCM-concentration effect. Centrifugation of said samples did not produce a resuspendable precipitate; even when centrifugation was skipped in sample preparation, insoluble CCM quickly precipitated. This contrasts with the $n_{\text{BSA}}:n_{\text{CCM}} = 1:20$ sample ratio sample, whose precipitate after centrifugation was quickly resuspended to its original state. The apparent high optical density of the solution with ratio $n_{\text{BSA}}:n_{\text{CCM}} = 1:4$ in Fig. 8b introduces the possibility of a suspension being present in the sample. However, this contradicts with our findings from native-PAGE that did not show BSA depletion. Overall, these results revealed the distinct outcomes obtained using different CCM concentrations in this protocol.

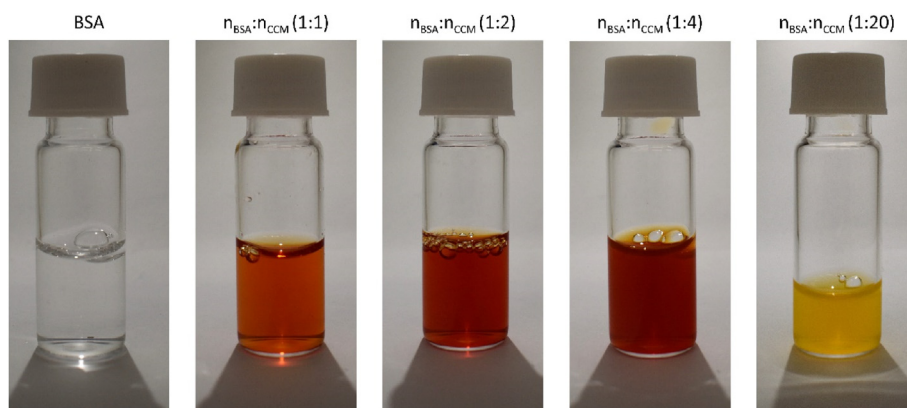


Fig. 8. The effect of the $n_{\text{BSA}}:n_{\text{CCM}}$ ratio on the outcome of homogenization. Sample labeled “BSA” did not contain CCM but was otherwise processed in the same manner as the CCM-containing samples. All samples were sonicated for 5 min during preparation. Examined $n_{\text{BSA}}:n_{\text{CCM}}$ ratios include: 1:1, 1:2, 1:4 and 1:20. The $n_{\text{BSA}}:n_{\text{CCM}} = 1:20$ sample required the use of a lower initial BSA concentration (5 mg/mL) to maintain the water/dichloromethane volume ratio.

4. Overall discussion

In order to verify that BSA-CCM association was responsible for the increased CCM content in the produced aqueous solutions, it was necessary to determine any potential self-assembly of the protein. Native-PAGE, and DLS data suggest that BSA aggregation beyond that of the commercial lyophilized BSA, was insignificant, if at all present in the samples. Moreover, near-equimolar ratios of BSA and CCM such as those used here, were not likely to favor NP formation; similar two-phase systems used for NP generation require an abundance of the hydrophobic compound to form a hydrophobic core which is then surrounded by intermolecularly crosslinked albumin molecules [25,50]. The centrifugation step for the removal of insoluble CCM rendered NP detection difficult since they would have been precipitated along with insoluble CCM. Nevertheless, the lack of BSA depletion in native-PAGE, combined with the fact that most of the originally added BSA (80–90%) was found in the produced solution, suggest BSA-CCM association rather than NP formation. This deduction was supported by the generation of a NP suspension in the sample with a $n_{\text{BSA}}:n_{\text{CCM}}$ ratio of 1:20, capable of staying in suspension for more than 48 h at 4 °C. Although this was expected based on the extensive literature on NAB iterations, the results from using near-equimolar $n_{\text{BSA}}:n_{\text{CCM}}$ ratios in sample preparations were not. CCM is known to naturally associate with BSA through hydrophobic and hydrophilic interactions [22] and recent studies of BSA-CCM association have determined the existence of ~ 1 binding site for CCM. Here, the association of more than one CCM molecule per BSA is corroborated by CCM quantification and CD data. Overall, we suspect that the association of CCM with BSA is enhanced in a two-step manner: initially, the water-immiscible dichloromethane facilitates the access of CCM to one or more hydrophobic pockets of BSA, which is then further assisted by the additional sonication step. The mechanism of this association remains to be determined however, while additional work is necessary to fully elucidate the nature of BSA-CCM interaction achieved by this method.

5. Conclusions

We have reported on a method that facilitates the association of CCM with BSA and produces aqueous solutions with high CCM content. All samples prepared in the described manner revealed a correlation between initial and final CCM contents. However, samples that were submitted to an intermediate sonication step showed higher CCM concentrations in the resulting aqueous solutions, compared to samples that were only submitted to the rapid mixing of the two-phase system by vortex mixer. BSA-CCM association was verified by the detection of an

ICD signal in the studies, and by the quenching of BSA fluorescence, which suggested CCM association localized in the vicinity of a Trp residue. Our approach was also aimed towards minimal disruption of the structure and disulfide bonds of BSA. Sonication provided an easy means of homogenizing the initial two-phase system while minimizing the application of shearing forces on BSA, and therefore avoiding the generation of intermolecular disulfide bridges and subsequent BSA oligomerization. Furthermore, short sonication of BSA has a minimal effect on its secondary structure [26]. Indeed, the evaluation of the secondary structure of BSA by CD showed minor CCM-dependent α -helix to β -sheet transitions, with the sonicated sample of $n_{\text{BSA}}:n_{\text{CCM}} = 1:4$ displaying the greatest transition, although α -helices remained dominant in all samples.

We expect this work to lead to the development of more advanced non-covalent albumin carriers which could include compounds of pharmacological interest, as well as proteins and peptides that have been conjugated with an albumin binder. Such systems should bypass the issue of colloidal instability associated with protein-based NPs and increase circulation times. Overall, this work has highlighted a simple and underexplored process to achieve protein-compound association with a potential importance to future drug-delivery applications.

Declaration of competing interest

The authors declare that they have no known competing financial interests or personal relationships that could have appeared to influence the work reported in this paper.

Acknowledgements

This work was financially supported by the project “CO2-Bio-Products” (MIS 5031682), which is funded by the Operational Program “Competitiveness, Entrepreneurship and Innovation” (NSRF 2014–2020) and co-financed by Greece and the EU (European Regional Development Fund). B.K. acknowledges the Erasmus+ program. We also acknowledge the valuable assistance of Georgios T. Sotiroudis in HPLC experiments.

Appendix A. Supplementary data

Supplementary data to this article can be found online at <https://doi.org/10.1016/j.jciso.2022.100051>.

References

- [1] T. Cedervall, I. Lynch, S. Lindman, T. Berggard, E. Thulin, H. Nilsson, K.A. Dawson, S. Linse, Understanding the nanoparticle-protein corona using methods to quantify exchange rates and affinities of proteins for nanoparticles, *Proc. Natl. Acad. Sci. Unit. States Am.* 104 (2007) 2050–2055, <https://doi.org/10.1073/pnas.0608582104>.
- [2] M.J. Mitchell, M.M. Billingsley, R.M. Haley, M.E. Wechsler, N.A. Peppas, R. Langer, Engineering precision nanoparticles for drug delivery, *Nat. Rev. Drug Discov.* 20 (2021) 101–124, <https://doi.org/10.1038/s41573-020-0090-8>.
- [3] K. Park, Facing the truth about nanotechnology in drug delivery, *ACS Nano* 7 (2013) 7442–7447, <https://doi.org/10.1021/nn404501g>.
- [4] Y. Xin, M. Yin, L. Zhao, F. Meng, L. Luo, Recent progress on nanoparticle-based drug delivery systems for cancer therapy, *Cancer Biol. Med.* 14 (2017) 228–241, <https://doi.org/10.20892/j.issn.2095-3941.2017.0052>.
- [5] M. Gaber, W. Medhat, M. Hany, N. Saher, J.-Y. Fang, A. Elzoghby, Protein-lipid nanohybrids as emerging platforms for drug and gene delivery: challenges and outcomes, *J. Contr. Release* 254 (2017) 75–91, <https://doi.org/10.1016/j.jconrel.2017.03.392>.
- [6] M. Lundqvist, J. Stigler, T. Cedervall, T. Berggård, M.B. Flanagan, I. Lynch, G. Elia, K. Dawson, The evolution of the protein corona around nanoparticles: a test study, *ACS Nano* 5 (2011) 7503–7509, <https://doi.org/10.1021/nn202458g>.
- [7] C. Saraiva, C. Praça, R. Ferreira, T. Santos, L. Ferreira, L. Bernardino, Nanoparticle-mediated brain drug delivery: overcoming blood-brain barrier to treat neurodegenerative diseases, *J. Contr. Release* 235 (2016) 34–47, <https://doi.org/10.1016/j.jconrel.2016.05.044>.
- [8] Y. Wei, Y. Sun, J. Wei, X. Qiu, F. Meng, G. Storm, Z. Zhong, Selective transferrin coating as a facile strategy to fabricate BBB-permeable and targeted vesicles for potent RNAi therapy of brain metastatic breast cancer in vivo, *J. Contr. Release* 337 (2021) 521–529, <https://doi.org/10.1016/J.JCONREL.2021.07.048>.
- [9] K.B. Johnsen, M. Bak, F. Melander, M.S. Thomsen, A. Burkhart, P.J. Kempen, T.L. Andresen, T. Moos, Modulating the antibody density changes the uptake and

- transport at the blood-brain barrier of both transferrin receptor-targeted gold nanoparticles and liposomal cargo, *J. Contr. Release* 295 (2019) 237–249, <https://doi.org/10.1016/j.jconrel.2019.01.005>.
- [10] P. Yousefpour, A. Varanko, R. Subrahmanyam, A. Chilkoti, Recombinant fusion of glucagon-like peptide-1 and an albumin binding domain provides glycemic control for a week in diabetic mice, *Adv. Ther.* 3 (2020), 2000073, <https://doi.org/10.1002/adtg.202000073>.
- [11] P. Yousefpour, L. Ahn, J. Tewksbury, S. Saha, S.A. Costa, J.J. Bellucci, X. Li, A. Chilkoti, Conjugate of doxorubicin to albumin-binding peptide outperforms doxorubicin, *Small* 15 (2019), 1804452, <https://doi.org/10.1002/sml.201804452>.
- [12] M. Martins, A. Loureiro, N.G. Azoia, C. Silva, A. Cavaco-Paulo, Protein formulations for emulsions and solid-in-oil dispersions, *Trends Biotechnol.* 34 (2016) 496–505, <https://doi.org/10.1016/j.tibtech.2016.03.001>.
- [13] A.O. Elzoghby, W.M. Samy, N.A. Elgindy, Albumin-based nanoparticles as potential controlled release drug delivery systems, *J. Contr. Release* 157 (2012) 168–182, <https://doi.org/10.1016/j.jconrel.2011.07.031>.
- [14] Z. Wen, F. Liu, G. Liu, Q. Sun, Y. Zhang, M. Muhammad, Y. Xu, H. Li, S. Sun, Assembly of multifunction dyes and heat shock protein 90 inhibitor coupled to bovine serum albumin in nanoparticles for multimodal photodynamic/ photothermal/chemo-therapy, *J. Colloid Interface Sci.* 590 (2021) 290–300, <https://doi.org/10.1016/j.jcis.2021.01.052>.
- [15] Q. Fu, J. Sun, W. Zhang, X. Sui, Z. Yan, Z. He, Nanoparticle albumin - bound (NAB) technology is a promising method for anti-cancer drug delivery, *Recent Pat. Anti-Cancer Drug Discov.* 4 (2009) 262–272, <https://doi.org/10.2174/157489209789206869>.
- [16] W.J. Gradishar, Albumin-bound paclitaxel: a next-generation taxane, *Expert Opin. Pharmacother.* 7 (2006) 1041–1053, <https://doi.org/10.1517/14656566.7.8.1041>.
- [17] F. Kratz, Albumin as a drug carrier: design of prodrugs, drug conjugates and nanoparticles, *J. Contr. Release* 132 (2008) 171–183, <https://doi.org/10.1016/j.jconrel.2008.05.010>.
- [18] E.N. Hoogenboezem, C.L. Duvall, Harnessing albumin as a carrier for cancer therapies, *Adv. Drug Deliv. Rev.* 130 (2018) 73–89, <https://doi.org/10.1016/j.addr.2018.07.011>.
- [19] Y. Wang, A. Lomakin, S. Kanai, R. Alex, S. Belli, M. Donzelli, G.B. Benedek, The molecular basis for the prolonged blood circulation of lipidated incretin peptides: peptide oligomerization or binding to serum albumin? *J. Contr. Release* 241 (2016) 25–33, <https://doi.org/10.1016/j.jconrel.2016.08.035>.
- [20] L.A. Ryberg, P. Sønderby, J.T. Bukrinski, P. Harris, G.H.J. Peters, Investigations of albumin–insulin Detemir complexes using molecular dynamics simulations and free energy calculations, *Mol. Pharm.* 17 (2020) 132–144, <https://doi.org/10.1021/acs.molpharmaceut.9b00839>.
- [21] M. Kuhlmann, J.B.R. Hamming, A. Voldum, G. Tsakiridou, M.T. Larsen, J.S. Schmökel, E. Sohn, K. Bienk, D. Schaffert, E.S. Sørensen, J. Wengel, D.M. Dupont, K.A. Howard, An albumin-oligonucleotide assembly for potential combinatorial drug delivery and half-life extension applications, *Mol. Ther. Nucleic Acids* 9 (2017) 284–293, <https://doi.org/10.1016/j.omtn.2017.10.004>.
- [22] P. Bourassa, C.D. Kanakis, P. Tarantilis, M.G. Poulissiou, H.A. Tajmir-Riahi, Resveratrol, genistein, and curcumin bind bovine serum albumin, *J. Phys. Chem. B* 114 (2010) 3348–3354, <https://doi.org/10.1021/jp9115996>.
- [23] N.P. Desai, C. Tao, A. Yang, L. Louie, Z. Yao, P. Soon-Shiong, S. Magdassi, US, 6749868 - protein stabilized pharmacologically active agents, and methods for the use thereof, *Magn. Reson. Imag.* 5 (1999), 916,596.
- [24] I.A. Hassanin, A.O. Elzoghby, Self-assembled non-covalent protein-drug nanoparticles: an emerging delivery platform for anti-cancer drugs, *Expert Opin. Drug Deliv.* 17 (2020) 1437–1458, <https://doi.org/10.1080/17425247.2020.1813713>.
- [25] T.H. Kim, H.H. Jiang, Y.S. Youn, C.W. Park, K.K. Tak, S. Lee, H. Kim, S. Jon, X. Chen, K.C. Lee, Preparation and characterization of water-soluble albumin-bound curcumin nanoparticles with improved antitumor activity, *Int. J. Pharm.* 403 (2011) 285–291, <https://doi.org/10.1016/j.ijpharm.2010.10.041>.
- [26] İ. Gülseren, D. Güzey, B.D. Bruce, J. Weiss, Structural and functional changes in ultrasonicated bovine serum albumin solutions, *Ultrason. Sonochem.* 14 (2007) 173–183, <https://doi.org/10.1016/j.ultsonch.2005.07.006>.
- [27] J. Jing Fu, C. Sun, Z. feng Tan, G. yao Zhang, G. bing Chen, L. Song, Nanocomplexes of curcumin and glyated bovine serum albumin: the formation mechanism and effect of glycation on their physicochemical properties, *Food Chem.* 368 (2022), 130651, <https://doi.org/10.1016/j.foodchem.2021.130651>.
- [28] A. Bujacz, K. Zielinski, B. Sekula, Structural studies of bovine, equine, and leporine serum albumin complexes with naproxen, *Proteins Struct. Funct. Bioinf.* 82 (2014) 2199–2208, <https://doi.org/10.1002/prot.24583>.
- [29] S. Falke, K. Dierks, C. Blanchet, M. Graewert, F. Cipriani, R. Meijers, D. Svergun, C. Betzel, Multi-channel in situ dynamic light scattering instrumentation enhancing biological small-angle X-ray scattering experiments at the PETRA III beamline P12, *J. Synchrotron Radiat.* 25 (2018) 361–372, <https://doi.org/10.1107/S1600577517017568>.
- [30] A. Bujacz, Structures of bovine, equine and leporine serum albumin, *Acta Crystallogr. Sect. D Biol. Crystallogr.* 68 (2012) 1278–1289, <https://doi.org/10.1107/S0907444912027047>.
- [31] B.T. Kurien, Y. Dorri, R.H. Scofield, Spicy SDS-PAGE gels: curcumin/turmeric as an environment-friendly protein stain, *Methods Mol. Biol.* 869 (2012) 567–578, https://doi.org/10.1007/978-1-61779-821-4_51.
- [32] M.L. Armstrong, Spherical gold nanoparticles impede the function of bovine serum albumin in vitro: a new consideration for studies in nanotoxicology, *J. Nanomater. Mol. Nanotechnol.* (2013), <https://doi.org/10.4172/2324-8777.1000124>, 02.

- [33] C. Li, T. Arakawa, Application of native polyacrylamide gel electrophoresis for protein analysis: bovine serum albumin as a model protein, *Int. J. Biol. Macromol.* 125 (2019) 566–571, <https://doi.org/10.1016/j.ijbiomac.2018.12.090>.
- [34] T. Peters, Serum albumin, *Adv. Protein Chem.* 37 (1985) 161–245, [https://doi.org/10.1016/S0065-3233\(08\)60065-0](https://doi.org/10.1016/S0065-3233(08)60065-0).
- [35] Y. Moriyama, D. Ohta, K. Hachiya, Y. Mitsui, K. Takeda, Fluorescence behavior of tryptophan residues of bovine and human serum albumins in ionic surfactant solutions: a comparative study of the two and one tryptophan(s) of bovine and human albumins, *J. Protein Chem.* 15 (1996) 265–272, <https://doi.org/10.1007/BF01887115>.
- [36] P.N. Naik, S.A. Chimatadar, S.T. Nandibewoor, Interaction between a potent corticosteroid drug - dexamethasone with bovine serum albumin and human serum albumin: a fluorescence quenching and fourier transformation infrared spectroscopy study, *J. Photochem. Photobiol. B Biol.* 100 (2010) 147–159, <https://doi.org/10.1016/j.jphotobiol.2010.05.014>.
- [37] M. Yang, Y. Wu, J. Li, H. Zhou, X. Wang, Binding of curcumin with bovine serum albumin in the presence of ι-carrageenan and implications on the stability and antioxidant activity of curcumin, *J. Agric. Food Chem.* 61 (2013) 7150–7155, <https://doi.org/10.1021/jf401827x>.
- [38] R. Starosta, F.C. Santos, R.F.M. de Almeida, Human and bovine serum albumin time-resolved fluorescence: tryptophan and tyrosine contributions, effect of DMSO and rotational diffusion, *J. Mol. Struct.* 1221 (2020), 128805, <https://doi.org/10.1016/j.molstruc.2020.128805>.
- [39] J.R. Lakowicz, Protein fluorescence, in: J.R. Lakowicz (Ed.), *Principles of Fluorescence Spectroscopy*, Springer US, Boston, MA, 1983, pp. 341–381, https://doi.org/10.1007/978-1-4615-7658-7_11.
- [40] V.D. Suryawanshi, L.S. Walekar, A.H. Gore, P.V. Anbhule, G.B. Kolekar, Spectroscopic analysis on the binding interaction of biologically active pyrimidine derivative with bovine serum albumin, *J. Pharm. Anal.* 6 (2016) 56–63, <https://doi.org/10.1016/j.jpha.2015.07.001>.
- [41] S.R. Hsieh, P.M. Reddy, C.J. Chang, A. Kumar, W.C. Wu, H.Y. Lin, Exploring the behavior of bovine serum albumin in response to changes in the chemical composition of responsive polymers: experimental and simulation studies, *Polymers* 8 (2016), <https://doi.org/10.3390/polym8060238>.
- [42] L.-Y. Zhu, G.-Q. Li, F.-Y. Zheng, Interaction of bovine serum albumin with two alkylimidazolium-based ionic liquids investigated by microcalorimetry and circular dichroism, *J. Biophys. Chem.* (2011) 147–152, <https://doi.org/10.4236/jbpc.2011.22018,02>.
- [43] J. Yu, Y. Chen, L. Xiong, X. Zhang, Y. Zheng, Conductance changes in bovine serum albumin caused by drug-binding triggered structural transitions, *Materials* 12 (2019) 1022, <https://doi.org/10.3390/ma12071022>.
- [44] D. Tedesco, C. Bertucci, Induced circular dichroism as a tool to investigate the binding of drugs to carrier proteins: classic approaches and new trends, *J. Pharm. Biomed. Anal.* 113 (2015) 34–42, <https://doi.org/10.1016/j.jpba.2015.02.024>.
- [45] A.C. Pulla Reddy, E. Sudharshan, A.G. Appu Rao, B.R. Lokesh, Interaction of curcumin with human serum albumin—a spectroscopic study, *Lipids* 34 (1999) 1025–1029, <https://doi.org/10.1007/s11745-999-0453-x>.
- [46] F. Zsila, Z. Bikádi, M. Simonyi, Unique, pH-dependent biphasic band shape of the visible circular dichroism of curcumin–serum albumin complex, *Biochem. Biophys. Res. Commun.* 301 (2003) 776–782, [https://doi.org/10.1016/S0006-291X\(03\)00030-5](https://doi.org/10.1016/S0006-291X(03)00030-5).
- [47] F. Zsila, Z. Bikádi, M. Simonyi, Molecular basis of the Cotton effects induced by the binding of curcumin to human serum albumin, *Tetrahedron Asymmetry* 14 (2003) 2433–2444, [https://doi.org/10.1016/S0957-4166\(03\)00486-5](https://doi.org/10.1016/S0957-4166(03)00486-5).
- [48] F. Zsila, Z. Bikadi, I. Fitos, M. Simonyi, Probing protein binding sites by circular dichroism spectroscopy, *Curr. Drug Discov. Technol.* 1 (2005) 133–153, <https://doi.org/10.2174/1570163043335135>.
- [49] F. Mohammadi, A.K. Bordbar, A. Divsalar, K. Mohammadi, A.A. Saboury, Analysis of binding interaction of curcumin and diacetylcurcumin with human and bovine serum albumin using fluorescence and circular dichroism spectroscopy, *Protein J.* 28 (2009) 189–196, <https://doi.org/10.1007/s10930-009-9184-1>.
- [50] M. Otagiri, V.T. Giam Chuang, Albumin in medicine: pathological and clinical applications, *Albumin Med. Pathol. Clin. Appl.* (2016) 1–277, <https://doi.org/10.1007/978-981-10-2116-9>.